International Journal of Nanomedicine

Dovepress
open access to scientific and medical research

Open Access Full Text Article

ORIGINAL RESEARCH

Dual-Sensitive Carbohydrate-Based Nanosystem for Targeted Drug Delivery to Potentiate the Therapeutic Efficacy of Ulcerative Colitis

Yuan Wang, Xiaoyu Song, Ru Cui, Xinlin Luo, Juntian Dong, Hanqi Wang, Chengcheng Song, Yifa Zhou, Sisi Cui

Engineering Research Center of Glycoconjugates, Ministry of Education, Jilin Provincial Key Laboratory of Chemistry and Biology of Changbai Mountain Natural Drugs, School of Life Sciences, Northeast Normal University, Changchun, 130024, People's Republic of China

Correspondence: Sisi Cui, Engineering Research Center of Glycoconjugates of Ministry of Education, Jilin Provincial Key Laboratory on Chemistry and Biology of Changbai Mountain Natural Drugs, School of Life Sciences, Northeast Normal University, Changchun, 130024, People's Republic of China, Email cuiss100@nenu.edu.cn

Purpose: Conventional oral formulations for inflammatory bowel disease (IBD) treatment are less than satisfactory, due to the poor controllability of drug release and lack of specificity to the inflammation sites in the gastrointestinal (GI) tract. To overcome these limitations, we developed a multiple carbohydrate-based nanosystem with pH/ROS dual responsibility and charge-mediated targeting ability for IBD-specific drug delivery.

Methods: In view of the overproduction of ROS and overexpression of cationic proteins in the inflammatory colon, the designed nanosystem was composed of oxidation-sensitive cyclodextrin (OX-CD), chitosan (CS) and pectin (AHP). OX-CD was utilized to load dexamethasone (DM) by the solvent evaporation method. CS and AHP with opposite charges were sequentially coated onto OX-CD to generate the nanosystems by the electrostatic self-assembly method. The physicochemical properties, stability, dual-sensitive drug release behavior, cytotoxicity, cellular uptake and anti-inflammatory activity were investigated in vitro. In vivo bio-distribution and therapeutic efficacy of the nanosystem were further evaluated in the ulcerative colitis (UC) mice.

Results: The obtained AHP/CS/OX-CD-DM nanosystem (ACOC-DM) could maintain stability under the GI pH environments, and release drug in the inflammatory colon with pH/ROS sensitivity. Dual polysaccharide-coated ACOC-DM exhibited higher cellular uptake and anti-inflammatory efficacy in macrophages than single polysaccharide-coated CS/OX-CD-DM nanosystem (COC-DM). Orally administrated ACOC-DM could enhance inflammation targeting ability and therapeutic efficacy of DM in the UC mice.

Conclusion: This carbohydrate-based nanosystem with pH/ROS dual sensitivity and inflammation targeting capacity may serve as a safe and versatile nanoplatform for IBD therapy.

Keywords: PH/ROS sensitivity, pectin, chitosan, oxidation-sensitive cyclodextrin, inflammation targeting, oral delivery

Introduction

Inflammatory bowel disease (IBD), which mainly encompasses ulcerative colitis (UC) and Crohn's disease (CD), is a group of chronic intestinal inflammatory diseases that are characterized pathologically by intestinal inflammation and epithelial injury. IBD is becoming globally prevalent, and more than 6.8 million people worldwide suffer from the complications of IBD.[1] Nevertheless, a curative treatment for IBD is still lacking, since the exact etiology remains obscure. Current treatment approaches involve the daily administration of high doses of aminosalicylates, antibiotics, corticosteroids, and immunosuppressants, with the aim of relieving acute attacks and preventing relapse episodes.[2] However, the delivery of free drugs using conventional formulations is insufficient and inadequate, owing to the poor controllability of drug release and lack of specificity to the inflammation sites in the gastrointestinal (GI) tract.[3,4] Numerous researches have reported that IBD patients have experienced decreasing efficacy over repeated administrations

Received: 11 June 2024
Accepted: 6 August 2024
Published: 21 August 2024

Graphical Abstract

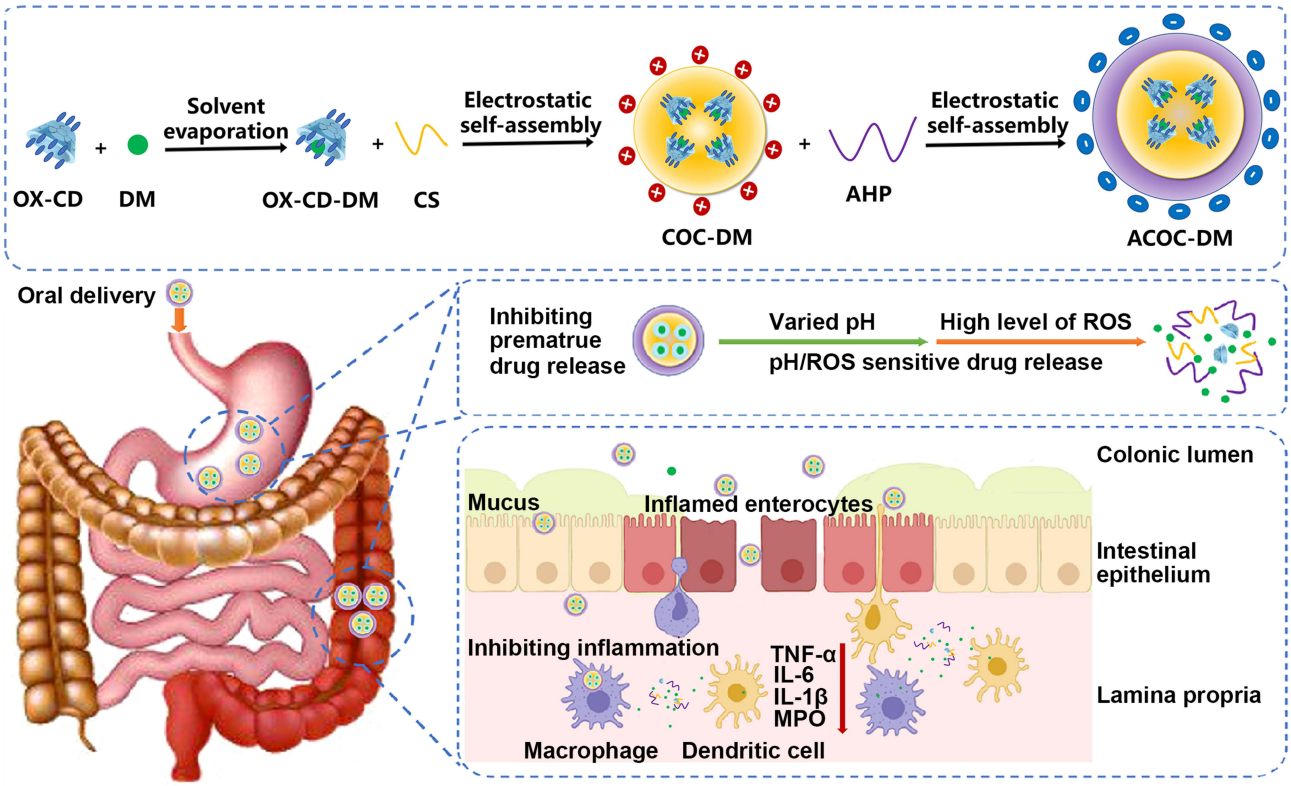

and suffered several side effects due to systemic drug absorption.[5–7] To enhance the therapeutic efficacy and minimize the systemic adverse effects, a disease-targeted drug delivery approach is desired for IBD treatment.[8–11]

Synthetic or natural polymer-based bio-responsive nanosystems enable targeted delivery of drugs to the inflammatory regions in the GI tract.[12,13] For instance, Jin et al developed an innovative H_2S-releasing nanoformulation by electrostatically adsorbing diallyl trisulfide-loaded peptide dendrimer nanogels onto the montmorillonite surface, which can effectively alleviate UC by eliminating reactive oxygen species (ROS), repairing the mucosal barrier and remodelling the gut microbiota.[14] Compared to synthetic polymers, natural polysaccharides possess great potential as candidate drugs or carrier materials for IBD treatment.[15–17] Polysaccharides can regulate major proinflammatory signalling pathways, protect intestinal barrier, modulate immunity, and balance the intestinal flora owing to their intrinsic anti-inflammatory, healing, macrophage-targeting and immunomodulatory activity.[16,18] On the other hand, natural polysaccharides have been extensively employed as micro/nano-carriers for IBD-targeted drug delivery, because of their non-toxicity, abundance in nature, stability in the stomach and biodegradability in the colon by the bacterial flora.[18] However, conventionally natural polysaccharide carriers frequently result in premature release in the upper GI tract or poor specificity across inflammation regions.[19,20] Various modified polysaccharide carriers with bio-responsive drug release and targeting ability for oral drug delivery are being explored to further potentiate the therapeutic efficacy of IBD.[15,17,18]

In comparison to the healthy colon, some pathological changes occurred during active IBD, such as the pH, epithelium barrier function, gut microbiota composition, degradative enzymes, etc.[21] These differences are being contemplated for the development of apposite IBD-targeted macro/nano-carriers. The varying pH values in different intestinal segments and the polysaccharide degrading enzymes produced by the colonic bacteria can be harnessed to achieve pH or enzyme-responsive colon-targeted drug delivery by utilizing diverse polysaccharide carriers, like chitosan, pectins and alginates and their derivatives.[15,22,23] Studies also reveal that the concentration of mucosal reactive oxygen

species (ROS) in the inflammation tissues of IBD patients is approximately 10–100 times higher compared to the healthy patients, which accelerates the progression of IBD.[24] The atypically elevated levels of mucosal ROS could potentially be exploited as a selective feature to design ROS-responsive delivery systems for the accurate delivery of IBD therapeutics.[25–28] Wang's group developed the polyvinylpyrrolidone modified bismuth selenide nanodiscs and the tannic acid-zinc coordinated nanoparticles to eliminate reactive oxygen and nitrogen species (RONS) to alleviate IBD and promote intestinal mucosal healing.[29,30] Apart from the above-mentioned bio-responsive delivery strategies, size-dependent and charge-mediated targeting approaches have been extensively explored for efficient local drug delivery to the inflammatory sites in IBD. Owing to the increased intestinal permeability and disordered mucosal barrier in IBD, nano-delivery systems have the ability to pass through the epithelial barriers, be absorbed by the colon and immune cells and accumulate at the inflammatory sites. This enables size-dependent targeting of nano-delivery systems to be achieved via the epithelial enhanced permeability and retention (eEPR) effect.[21] Charge-mediated targeting is based on the fact that the surface of mucins is negatively charged, and several positively charged proteins like transferrin and eosinophil cationic proteins are overexpressed in the inflamed colon.[31,32] Therefore, positively charged polysaccharide delivery systems have the potential to interact with the oppositely charged mucous layer, whereas negatively charged polysaccharide delivery systems may preferentially interact with the abundant cationic proteins on the inflamed colonic surface through electrostatic interaction, thereby enhancing the retention of drugs in the inflammatory sites.[33,34]

Given the potential of bio-responsive polysaccharide nanocarriers for the targeted therapy of IBD, a multiple carbohydrate-based nanosystem with pH/ROS sensitivity and charged-mediated targeting ability were developed to deliver dexamethasone (DM) for UC treatment (Figure 1). Oxidation-sensitive cyclodextrin (OX-CD) modified with 4-(hydroxymethyl) phenylboronic acid pinacol ester (PBAP) was synthesized to load DM by the solvent evaporation method. Positively charged chitosan (CS) and negatively charged pectin (AHP) were sequentially combined with the OX-CD to form multiple polysaccharide-based nanosystems using the electrostatic self-assembly method. The physicochemical properties, pH/ROS dual-sensitive release profiles, gastrointestinal stability, cellular uptake, in vivo bio-distribution and therapeutic efficacy of the prepared nanosystem were evaluated for the treatment of UC.

Materials and Methods

Materials

Low-methoxyl pectin (AHP) was isolated from sunflower head residues and de-esterified according to our previously established procedures.[35,36] The plant species was identified by the botanist Dr. Mingzhou Sun (Northeast Normal University, China), and the voucher specimen was deposited in the Herbarium of Northeast Normal University (NENU). β-cyclodextrin (β-CD), fluorescein isothiocyanate (FITC) and Hoechst 33342 were purchased from Aladdin Reagents (Shanghai, China). Chitosan (Mw = 100 kDa, 80% deacetylated) and dexamethasone (DM) and were purchased from Meilune Biotech (Dalian, Liaoning, China). 4-(Hydroxymethyl) phenylboronic acid pinacol (PBAP), 4-dimethylaminopyridine (DMAP) and 1,1'-carbonyldiimidazole (CDI) were obtained from Rhawn Reagent (Shanghai, China). Anhydrous dimethylsulfoxide and dichloromethane were provided by J & K Scientific (Beijing, China). 3-(4, 5-dimethyl-2-thiazolyl)-2, 5-diphenyl-2-H-tetrazolium bromide (MTT) were purchased from Dingguo Biotech (Beijing, China). Lipopolysaccharide was provided by Sigma–Aldrich (St Louis, MO, USA). Griess reagent was obtained from Beyotime Institute of Biotechnology (Shanghai, China). Dextran sulfate sodium (DSS, Mw = 40 kDa) was purchased

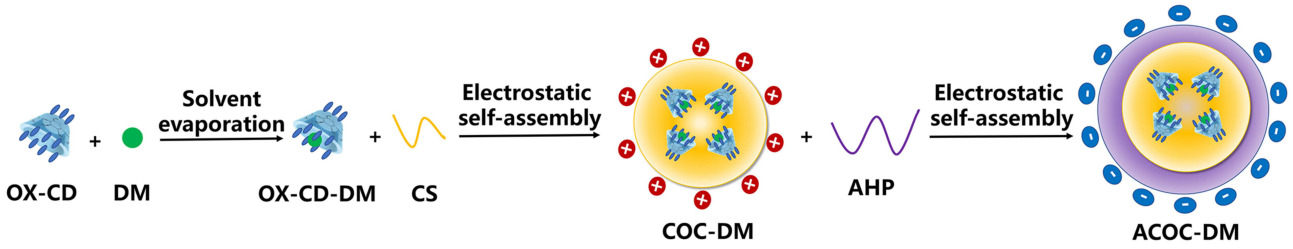

Figure 1 Scheme of the preparation of dual-sensitive carbohydrate-based nanosystems.

from Yuanye Bio-Technology (Shanghai, China). The mouse TNF-α, interleukin-6 (IL-6) and interleukin-1β (IL-1β) ELISA kit were supplied by BOSTER Biotechnology Inc. (Wuhan, China). Hydrogen peroxide (H_2O_2) and myeloperoxidase (MPO) activity assay kits were purchased from Nanjing Jiancheng Bioengineering Institute (Nanjing, China). Near-infrared fluorescent cyanine dye (Cy-Cl) was kindly gifted by Prof. Zhenwei Yuan (China Pharmaceutical University). All other chemical reagents were purchased from Beijing Chemical Works (Beijing, China) and used as received.

Fabrication of the Carbohydrate-Based Nanosystems

ROS-responsive β-CD (OX-CD) was synthesized using the previously reported procedure and characterized by ^{1}H NMR (BrukerAV-600, Bruker, Germany), Fourier transform infrared (FT-IR, Spectrum Two, PE, USA) and UV–Vis spectra (UV-2700, Shimadzu, Japan).[37] DM as a model drug was loaded into OX-CD by a solvent evaporation method. Briefly, OX-CD (10 mg) was dissolved in ddH_2O (2.5 mL), and then 0.5 mL of DM methanol solution (6.6 mg/mL) was added dropwise into the OX-CD solution under stirring. After stirring the mixture at room temperature for 5 h, the DM-loaded OX-CD dispersion was obtained by evaporation of methanol using a rotating evaporator. Thereafter, CS and AHP were sequentially coated onto DM-loaded OX-CD by an electrostatic self-assembly method, to prepare the CS-coated nanosystem (COC-DM) and AHP/CS-coated nanosystem (ACOC-DM). In detail, CS was dissolved in a 1% acetic acid solution to obtain a 0.5% solution and the pH was adjusted to 5.5 by slowly adding a NaOH solution (0.1 M). CS solution was then added into the DM-loaded OX-CD dispersion at different mass ratios of OX-CD to CS (2:1, 1:1 and 1:2). The mixture was sonicated by an ultrasound probe (Scientz-IID, China) and then magnetically stirred for 1 h. The COC-DM was collected by centrifugation (13000 rpm, 20 min), and re-dispersed in 5 mL ddH_2O. AHP was dissolved in ddH_2O (5 mg/mL) and de-esterified using 0.5 M NaOH at 4 °C for 4 h to produce de-esterified AHP (degree of esterification (DE) = 0%).[36] The de-esterified AHP aqueous solution (1.5% w/v) was slowly added into the COC-DM dispersion at different mass ratios of AHP to CS (1:2.5, 1:3 and 1:4) and further dispersed by sonication. After stirring for 0.5 h, the ACOC-DM was collected by centrifugation (13000 rpm, 20 min), washed with ddH_2O, and re-suspended in ddH_2O by sonication. For cell imaging and in vivo fluorescent imaging studies, FITC-loaded nanosystems or Cy-Cl loaded nanosystems were fabricated following the same procedure described above, except for using FITC or Cy-Cl to replace DM, in which the mass ratio of fluorescent dye to OX-CD was 1:4.

Characterization of the Carbohydrate-Based Nanosystems

Size distribution and zeta potential of the obtained nanosystems were measured by dynamic light scattering (DLS, NanoBrook Omni, Brookhaven, USA). The morphology of nanosystems was observed by a scanning electron microscope (SEM, XL-30 ESEM FEG, Micro FEI Philips) at an acceleration voltage of 20 kV after sputter-coating with gold for 120 s. The concentration of DM was determined by Waters e2695 high performance liquid chromatography (HPLC, Waters, USA) with the mobile phase composed of water and acetonitrile (volume ratio 65:35) at a flow rate of 1 mL/min. Waters symmetry C18 (4.6 × 150 mm, 5 μm) column was used as stationary phase. The injection volume of the samples was 20 μL and the detection wavelength was 240 nm. For the drug loading determination, 2 mg of nanosystems was accurately weighed and stirred in a mixture of 1.0 M of H_2O_2 (0.5 mL) and acetonitrile (0.5 mL) for 2 h until complete dissolution. The sample was centrifuged and the DM content in the supernatant was analyzed by HPLC. Drug loading efficiency (LE) and encapsulation efficiency (EE) were calculated by following equations: LE (%, w/w) = Weight of DM in the NPs/Total weight of NPs × 100%; EE (%, w/w) = Weight of DM in the NPs/Initial DM feeding weight × 100%.

H_2O_2-Responsive Degradation and Stability of Nanosystems

H_2O_2-responsive degradation of OX-CD was performed in 0.01 M PBS buffer (pH 7.4) containing various concentrations of H_2O_2 at 37 °C (0, 0.1, 0.25, 0.5 and 1.0 mM). Quantitative experiments were performed by measuring the absorbance of the NPs solution at 500 nm at various time points. Degradation rate was calculated by the following equation: Degradation rate% = $(A-A_\infty)/(A_0-A_\infty) \times 100\%$, where A_0 is the absorbance at 0 min, A is the absorbance at different time points, A_∞ is the absorbance when completely degraded.

To evaluate the stability of nanosystems in the solution, COC-DM and ACOC-DM dispersed in ddH_2O (1 mg/mL) were placed 4 °C for 30 d. The particle size and PDI of the solutions were measured every day. To study the stability of these nanosystems in the GI tract, the COC-DM and ACOC-DM were incubated in simulated gastric fluid (SGF, pH 1.2) containing pepsin and simulated colonic fluid (SCF, 0.01 M PBS at pH 7.4). After incubation, the morphology, size distribution and zeta potential of nanosystems were examined by SEM and DLS analysis, respectively. To assess the H_2O_2-responsibility of nanosystems in colon environment, COC-DM and ACOC-DM were dispersed in SCF with and without 1.0 mM H_2O_2 at room temperature. Digital photos of nanosystem dispersions were taken during hydrolysis for a direct illustration. After 24 h of incubation, the size distribution of nanosystems was measured by DLS analysis.

In vitro Drug Release

The release profiles of COC-DM and ACOC-DM were separately performed in SGF (pH 1.2), simulated small intestinal fluid (SIF, 0.01 M PBS at pH 6.8) and SCF (pH 7.4) without enzymes. To evaluate drug release in SGF and SIF, 10 mg of COC-DM or ACOC-DM in 1 mL ddH_2O was added into dialysis bags (MWCO = 1.0 kDa). The bags were incubated in 20 mL SGF at 37 °C with shaking for 2 h at 100 rpm. Then, the bags were transferred into 20 mL SGF and shaken for another 10 h. To investigate ROS-responsive drug release in colon pH, the dialysis bags containing 10 mg/mL nanosystem dispersions were, respectively, immersed into 20 mL SCF with and without 1.0 mM H_2O_2, and shaken (100 rpm) at 37 °C for 24 h. At specific time points, 1.0 mL of the release medium was withdrawn and the same volume of fresh medium was replenished. The amount of DM in the supernatant was quantified by HPLC.

Cell Studies

Cell Culture

Caco-2 (human epithelial colorectal adenocarcinoma cells) and RAW 264.7 (murine monocyte-macrophages) cell lines were purchased from the American Type culture collection (ATCC, USA). All cells were cultured in DMEM supplemented with 10% FBS and 1% penicillin/streptomycin, and incubated at 37 °C in an atmosphere with 90% relative humidity and 5% CO_2.

Cytotoxicity

The cytotoxicity of the blank nanosystems was assessed using the MTT assay. RAW 264.7 macrophages and Caco-2 cells were seeded onto 96-well culture plates at a density of 1×10^4 cells/well, respectively. After a 24-h culture, different amounts of COC (0.156, 0.312, 0.625, 1.25 mg/mL) and ACOC (0.312, 0.625, 1.25, 2.5 mg/mL) were added into cell medium (n = 5). After incubation for 24 h, 20 μL of MTT solution (5 mg/mL) was added into each well and incubated for another 4 h. Then, culture medium containing MTT was replaced by 150 μL of DMSO. The absorbance of the resultant solutions was measured at 570 nm using a plate reader (Tecan Infinite F50).

Cellular Uptake

Cellular uptake was performed on RAW 264.7 macrophages. The cells were seeded onto a 24-well culture plate at a density of 1×10^5 cells/well. After 24 h of cell attachment, 200 μL of FITC, COC-FITC and ACOC-FITC containing the same dose of FITC (0.05 mg/mL) were added in the culture medium. After incubation for 4 h, the cells were fixed in 4% paraformaldehyde for 20 min and washed three times with PBS. Cell nuclei were stained with Hoechst 33342 (5 μg/mL) for 30 min. After washing three times with PBS, the cells were imaged by a fluorescent microscope (IX71, Olympus, Japan).

In vitro Anti-Inflammatory Activity

RAW 264.7 macrophages were seeded onto on 96-well plates at the density of 1×10^4 cells/well. After 24 h culture, the cells were incubated without or with nanosystems (containing 40 μM of DM) and free DM (40 μM), stimulated with LPS at a final concentration of 500 ng/mL. After 24 h co-incubation, the supernatant in each well was collected and the presence of nitrite in cell medium was measured using the Griess reagent following the manufacturer's instructions. The levels of pro-inflammatory cytokines TNF-α and IL-6 were quantified with their corresponding ELISA kits.

Animal Studies

Dextran Sulfate Sodium-Induced UC Mouse Model

BALB/c (male, 20 ± 2 g) were purchased from Changchun Institute of Biological Products Co., Ltd. All animal experiments were conducted in compliance with the Animal Management Rules of the Ministry of Health of the People's Republic of China and approved by the Institutional Animal Care and Use Committee or the Animal Experimental Ethics Committee of Northeast Normal University. The UC mouse model was established by replacing the drinking water containing DSS (3.0%, w/v) for 7 d.

In vivo Fluorescence Imaging

DSS-induced UC mice were administrated with 0.2 mL of free Cy-Cl (0.25 mg/mL) or ACOC-Cy-Cl (containing 0.25mg/mL Cy-Cl) through oral administration. At the predetermined time points (0 min, 5 min, 30 min, 1 h, 2 h, 4 h, 6 h, 8 h, 24 h), mice were anesthetized. Distribution of ACOC-Cy-Cl or free Cy-Cl in the GI tract after oral administration was monitored using an in vivo imaging system (IVIS Lumina III, PerkinElmer, USA) with the excitation wavelength of 700 nm and emission wavelength of 790 nm. The mice were euthanized at 2 h, 4 h and 6 h after administration. The colon and the major organs (heart, liver, spleen, lung and kidney) of mice were isolated and blood samples were collected for fluorescence imaging, and the regional fluorescence intensities were analyzed by the software of IVIS.

In vivo Therapeutic Activity Against UC

BALB/c mice were randomly divided into 6 groups (n = 8), namely the control group, DSS model group, DM-0.5 group, ACOC-DM-0.1 group, ACOC-DM-0.25 group and ACOC-DM-0.5 group. Mice in the control group were given regular drinking water, while those in the other group were given 3.0% DSS in drinking water for 7 d. Meanwhile, mice in the treatment group received daily oral administration of ACOC-DM (containing 0.1, 0.25 and 0.5 mg/kg DM) or free DM (0.5 mg/kg) from day 3 to day 10. The body weight of mice was recorded daily throughout the experiments. The health conditions of mice were evaluated with the disease activity index (DAI), which mainly includes body weight loss (0−4), fecal bleeding (0−4), and stool consistency state (0−4). At day 10, the blood, colon, spleen and liver of mice were collected. The organ index was calculated using the following equation: Organ index = Organ weight (g) / Body weight (g) × 100%. The levels of IL-6, IL-1β, TNF-α, H_2O_2, and MPO activity in colonic tissues were measured with their corresponding commercial kits. For histological examination, the colon tissues were fixed in a 4% paraformaldehyde solution for 48 h and embedded in paraffin. Then, the tissues were sectioned at a thickness of 5 μm and stained with hematoxylin and eosin (H&E) followed by visualization under the fluorescent microscope (IX71, Olympus, Japan).

Statistical Analysis

All results were expressed as mean ± standard deviation (S.D). Statistical significance was assessed by the Student's *t*-test between two groups, and the level of significance was set at the probabilities of $*p < 0.05$, $**p < 0.01$, and $***p < 0.001$.

Results

Fabrication and Characterization of the Dual-Sensitive Carbohydrate-Based Nanosystems

To develop ROS-responsive materials, the boronic ester-conjugated β-CD (OX-CD) was synthesized using a previously reported procedure, and confirmed by ^{1}H NMR, FT-IR and UV-Vis spectroscopy.[37] The characteristic signals from PBAP could be distinctly observed in the ^{1}H NMR, FT-IR and UV-Vis spectroscopy of OX-CD (Figure 2A–C), which was consistent with the previous report.[37] Approximate 9 PBAP moieties were conjugated to each β-CD molecule, calculated on the basis of the ^{1}H NMR spectrum. Hydrolysis profiles of the as-synthesized OX-CD were studied in ddH_2O or ddH_2O containing 1.0 mM H_2O_2. Colloidal solutions could still be observed 6 h after incubation in ddH_2O at 37 °C, whereas the OX-CD solutions became clear at 60 min in the presence of H_2O_2, indicating the H_2O_2-responsive hydrolysis of OX-CD (Figure 2D). Quantitative study indicated that the degradation rate of OX-CD was dependent on the H_2O_2 concentration. A 98% of OX-CD could be hydrolyzed in the ddH_2O containing 1.0 mM H_2O_2 within 60 min, while only 4% of OX-CD was hydrolyzed in ddH_2O alone, further confirming the successful synthesis of ROS-responsive OX-CD (Figure 2E).

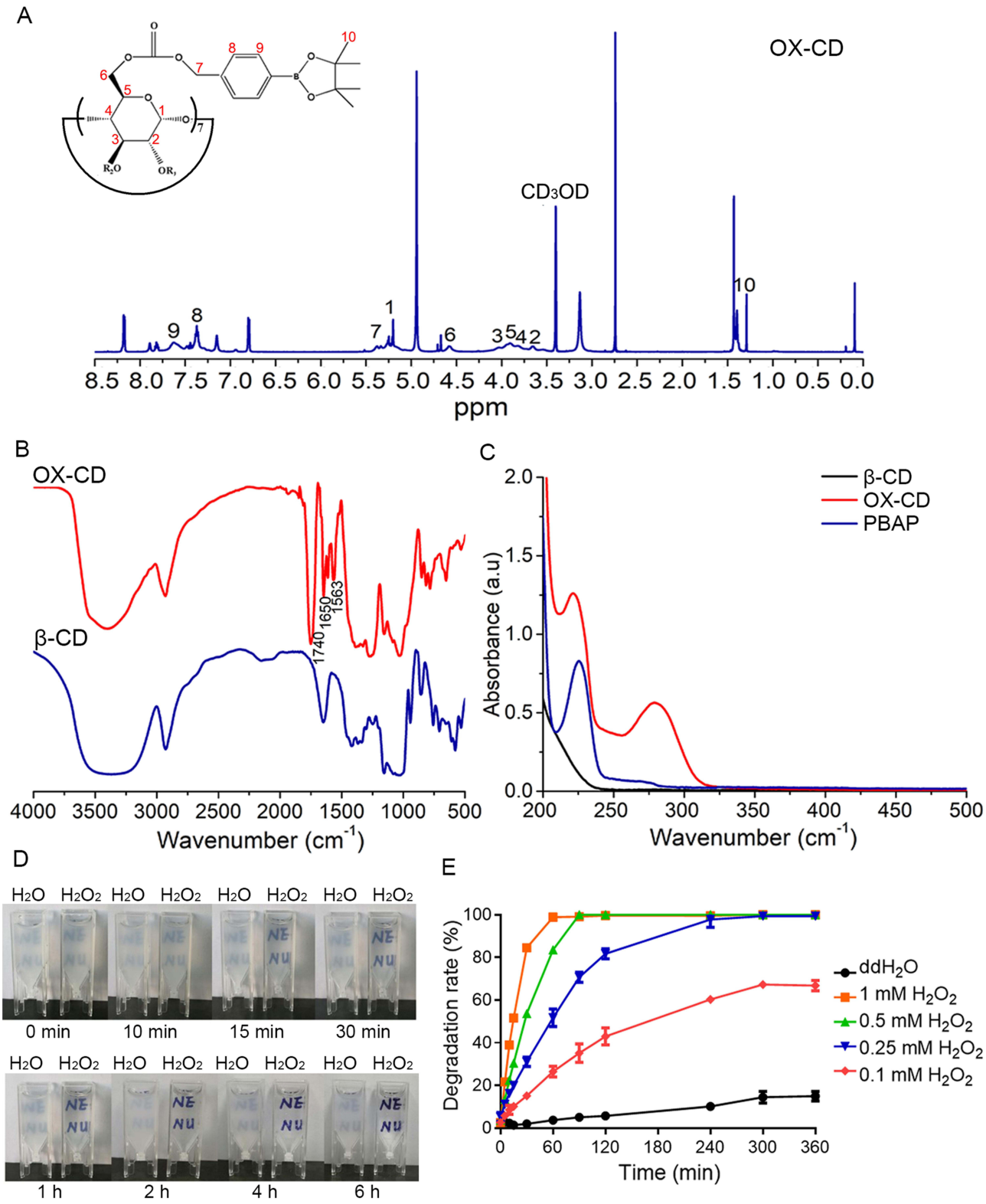

Figure 2 Characterization of OX-CD. (**A**) ^{1}H NMR spectra of OX-CD in CD_3OD. (**B**) FT-IR and (**C**) UV-Vis absorption spectra of OX-CD. (**D**) Photos of the appearance of OX-CD dispersion along with time after the addition of 1.0 mM H_2O_2. (**E**) Degradation curves of OX-CD dispersion at different H_2O_2 concentrations.

https://doi.org/10.2147/IJN.S472244 DovePress

DM as a model drug was loaded into the resulting OX-CD by a solvent evaporation method. Positively charged CS and negatively charged AHP were sequentially coated onto the DM-loaded OX-CD through electrostatic interaction (Figure 1). To optimize the size and surface charge, DM-loaded nanosystems were prepared at different OX-CD/CS and CS/AHP mass ratios. When the OX-CD/CS mass ratio reached 1/2, the obtained COC-DM possessed a comparatively smaller particle size (320.68 ± 8.16 nm, PDI = 0.18 ± 0.03, Figure 3A) and a higher zeta potential (+29.96 ± 2.18 mV, Figure 3B). After CS coating, surface charge of COC-DM changed from negative to positive as the increase of OX-CD/CS mass ratio from 2/1 to 1/2 (Figure 3B). AHP (DE = 0%) was then coated onto the COC-DM prepared at the OX-CD/CS mass ratio of 1/2. With the decrease of CS/AHP mass ratio from 1/2.5 to 1/4, the particle sizes of ACOC-DM were all larger than that of COC-DM, among which the smallest particle size was obtained with CS/AHP mass ratio of 1/3 (538.3 ± 22.9 nm, PDI = 0.29 ± 0.01, Figure 3C). The zeta potentials of ACOC-DM became more negative than −30 mV, when decreasing the CS/AHP mass ratio (Figure 3D).

At the fixed OX-CD/CS mass ratio of 1/2 and CS/AHP mass ratio of 1/3, the morphology of nanosystems observed by SEM showed that the COC-DM and ACOC-DM were spherical in shape (Figure 4A). The size of ACOC-DM (~500 nm) was larger than that of COC-DM (~300 nm), due to the presence of AHP layer on the surface of COC-DM. The average hydrodynamic diameter of ACOC-DM measured by DLS was increased to 538.32 ± 22.9 nm, compared to the COC-DM with a diameter of 320.68 ± 8.16 nm (Figure 4B). After AHP coating on the surface of COC-DM, the zeta potential of ACOC-DM was reversed from +29.96 ± 2.18 mV to −35.5 ± 0.5 mV (Figure 4B). The LE and EE of COC-DM were 8.7 ± 0.1% and 86.3 ± 1.2%, while the LE and EE of ACOC-DM was 3.1 ± 0.1% and 85.6 ± 2.2%,

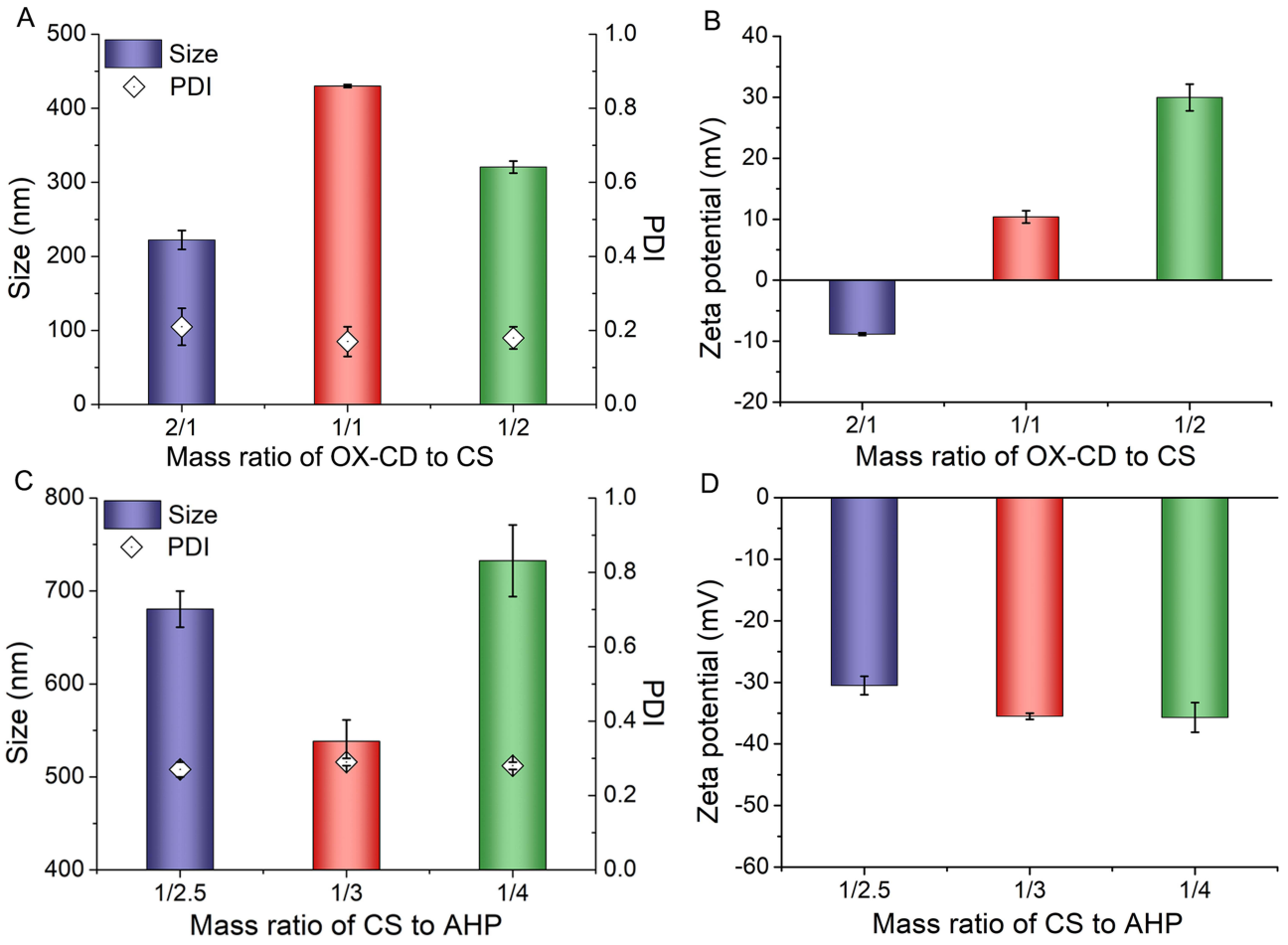

Figure 3 Influence of OX-CD/CS and CS/AHP mass ratios on particle size and zeta potential of the carbohydrate-based nanosystems. (**A**) Particle size and (**B**) zeta potential of nanosystems prepared at different OX-CD/CS mass ratios. (**C**) Particle size and (**D**) zeta potential of nanosystems prepared at different CS/AHP mass ratios.

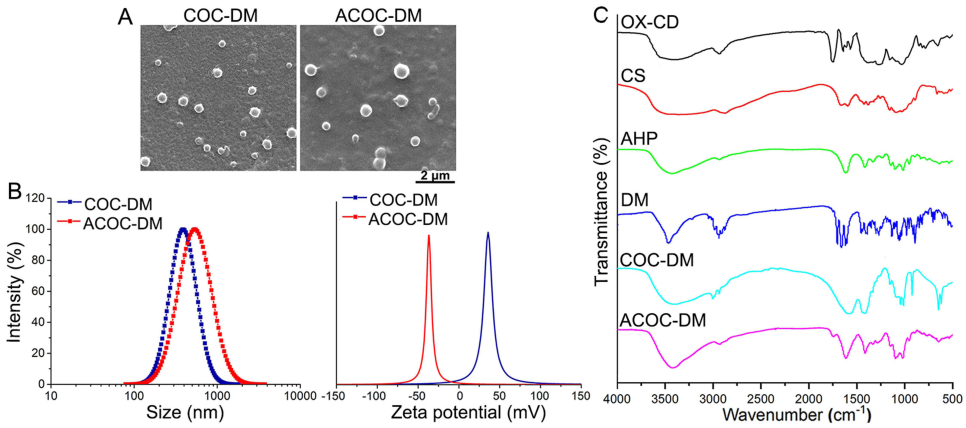

Figure 4 Characterization of dual-sensitive carbohydrate-based nanosystems. (**A**) SEM images, (**B**) particle size distribution and zeta potential, (**C**) FT-IR spectra of COC-DM and ACOC-DM.

respectively. The composition of nanosystems was confirmed by analysis of FTIR (Figure 4C). The bands ranging from 3000 to 2870 cm^{-1} in the COC-DM were attributed to the C−H stretching vibrations of the DM, OX-CD and CS. The broad band located around 1585 cm^{-1} was assigned to the amino group of CS. The band around 1413 cm^{-1} was attributed to the −OH bending vibration of CS and OX-CD. The characteristic bands of OX-CD, CS and DM were found with minor shift in the COC-DM, probably due to the hydrogen bonding interaction. In the FTIR spectrum of ACOC-DM, the characteristic peaks of non-esterified pectin at 1613 and 1413 cm^{-1} appeared, which was attributed to the C=O asymmetric and symmetric stretching in the -COOH group of AHP, indicating the presence of AHP coating.

In this study, we developed the pH/ROS dual-sensitive carbohydrate-based nanosystem for oral colon-targeted drug delivery, in order to potentiate the therapeutic efficacy, reduce systemic exposure and minimize side effects of free drugs for UC treatment. DM, which is a hydrophobic glucocorticoid with a poor colon targeting ability and extensive side effects, was selected as a model drug for UC therapy, since the prepared carbohydrate-based nanosystems are capable of loading hydrophobic drugs. DM was first loaded into the OX-CD core of nanosystems through solvent evaporation. As the PBAP situated at the rim of OX-CD may extend the hydrophobic cavity of β-CD, DM could be more easily included into the hydrophobic cavity of OX-CD after evaporation of methanol from methanol-water mixtures. After drug loading, DM-loaded OX-CD possessed a negative surface charge in water. Thereafter, the opposite charged CS and AHP were sequentially self-assembled onto the DM-loaded OX-CD via electrostatic interaction. To enhance the negative charge of ACOC-DM, we prepared de-esterified pectin (DE = 0%) using a homogalacturonan-type pectin with a DE of 34.5% and galacturonic acid content of 75%. ACOC-DM made of non-esterified pectin was able to form stable nanosystems in the range of CS/AHP mass ratio from 1/2.5 to 1/4. This is because it has more negatively charged carboxyl groups that could help prevent the nanosystem from aggregating in the solution. Although the surface charge of ACOC-DM become more negative as the increase of AHP content, drug loading may decrease with increased AHP content. Therefore, OX-CD/CS/AHP mass ratio was fixed at 1/2/6 to prepare nanosystems for further study.

Stability and ROS-Responsive Hydrolysis

Storage stability was evaluated by storing the nanosystem dispersions at 4 °C for a duration of 30 days. As shown in Figure 5A, the results demonstrate that the average size of ACOC-DM and COC-DM exhibited minimal variation during the 30-day period, indicating that these nanosystems had good stability for long-term storage. As the nanosystems are intended to transport drugs to colonic inflammation sites, these nanosystems should maintain stability during transit to the colon, and subsequently undergo degradation by the local ROS. We explored the stability and ROS-responsive hydrolysis of these nanosystems under the simulated GI conditions. In SGF (pH 1.2), the zeta potential of COC-DM dropped to +5.41 ± 1.31 mV, and particle size dramatically increased (Figure 5B and C). The aggregation and precipitation could be observed in SEM images and photographs of COC-DM dispersion, which confirmed that COC-DM had poor stability in

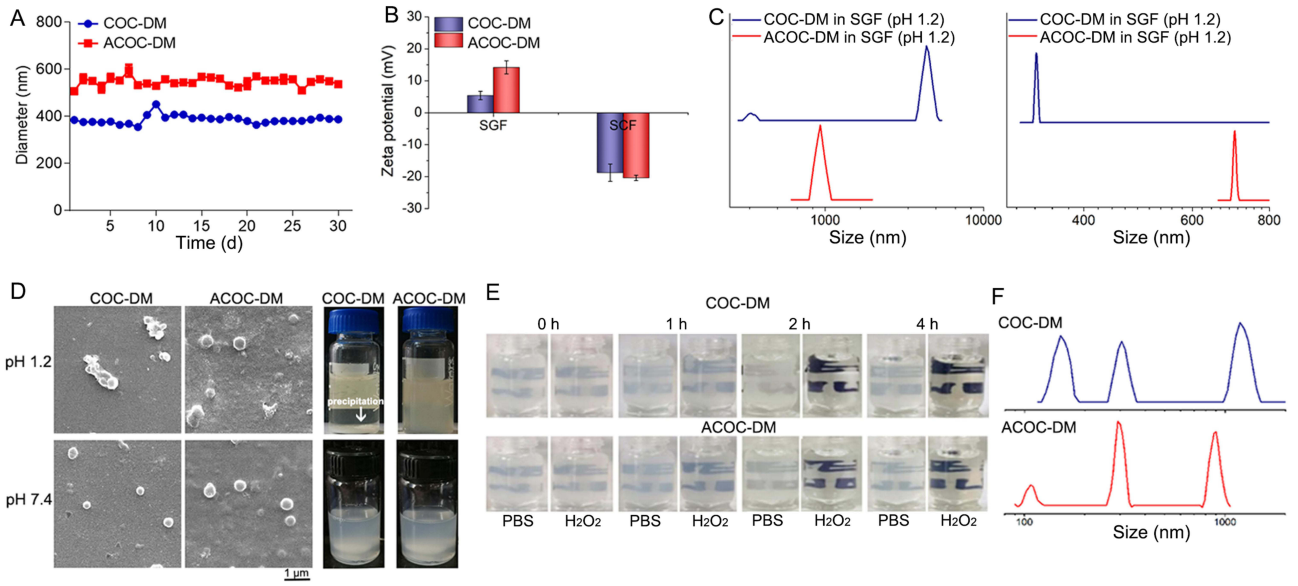

Figure 5 Stability and ROS-responsive hydrolysis of carbohydrate-based nanosystems. (**A**) Changes in particle size of nanosystems within 30 days. (**B**) Zeta potentials, (**C**) multimode size distribution, (**D**) SEM images and the appearance of COC-DM and ACOC-DM in SGF (pH 1.2) and SCF (pH 7.4). (**E**) The appearance of nanosystem in SCF (pH 7.4) without 1.0 mM H_2O_2. (**F**) Multimode size distribution of nanosystems after incubation in SCF containing 1.0 mM H_2O_2 for 24 h.

SGF (Figure 5D). In contrast, the zeta potential of ACOC-DM was +14.2 ± 2.05 mV higher than that of COC-DM, and the particle size only slightly increased in SGF (Figure 5B and C). Furthermore, SEM images and the appearance of ACOC-DM dispersion showed that ACOC-DM was more stable in SGF, suggesting that the stability of COC-DM was significantly improved after AHP coating (Figure 5D). In SCF (pH 7.4), both COC-DM and ACOC-DM exhibited a negative potential (−18.76 ± 2.7 mV and −20.38 ± 0.85 mV) and a narrow size distribution compared to that in SGF. There were no significant changes in the morphology and appearance of nanosystems after 24 h of incubation (Figure 5D). The H_2O_2-responsive hydrolysis of nanosystems was further investigated in SCF containing 1.0 mM H_2O_2, to mimic the high ROS concentration in the inflamed tissue of UC. The opalescent colloidal dispersions of COC-DM and ACOC-DM were almost clear after 4 h of incubation in SCF with H_2O_2 (Figure 5E). The size distribution of COC-DM and ACOC-DM became wide, and multiple peaks were observed after 24 h incubation in SCF with H_2O_2 (Figure 5F). These results indicated the ROS-responsive hydrolysis of nanosystems in the simulated colonic environment.

The stability results demonstrate that the AHP coating on the surface attenuates the tendency of COC-DM to aggregate in the upper GI tract, implying that the dual-polysaccharide coated ACOC-DM is more stable than the single-polysaccharide coated COC-DM in the upper GI tract. When incubated in SGF, the potential values of COC-DM decreased more than ACOC-DM. This may be due to the amino groups in CS are highly protonated in SGF, and therefore COC-DM are more likely to bind to pepsin to form a protein corona, resulting in the formation of larger self-aggregates with a broader size distribution.[38] After AHP coating, the carboxyl groups in pectin would electrostatically repel the negatively charged pepsin, thereby making ACOC-DM more stable in SGF. In SCF, both COC-DM and ACOC-DM show less negative potentials than that in water, owing to the deprotonation of amino groups in CS and the charge shielding effect of the salt ions. For ACOC-DM, the electrostatic interaction and hydrogen bonding of the two polysaccharides CS and AHP result in much tighter and more stable structures of nanosystems, which would be beneficial for maintaining their nanostructures before they arrive at the inflammation sites in the colon. Even though the AHP and CS coating on the OX-CD may, to some extent, reduce the ROS-responsive hydrolysis rate of the entire nanosystem, the majority of nanosystems might still be hydrolyzed when they remain in a high ROS environment such as the inflamed colon.

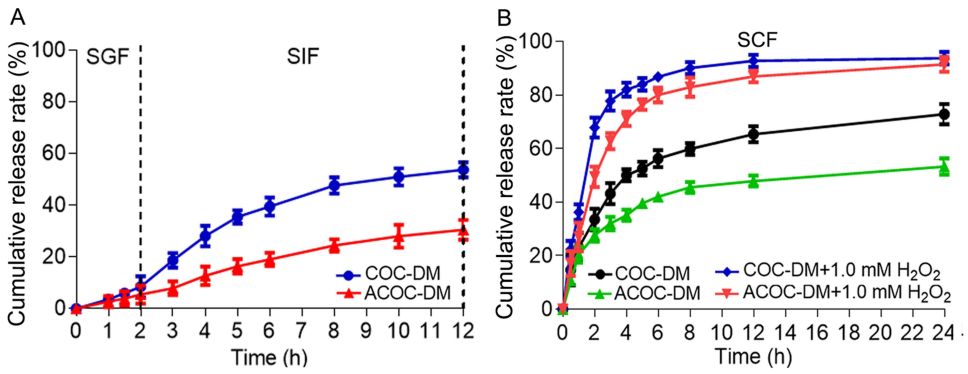

Figure 6 Drug release profiles of nanosystems. (**A**) DM release profiles from the nanosystems in SGF (HCl, pH 1.2) and SIF (PBS, pH 6.8). (**B**) DM release profiles from the nanosystems in SCF (PBS, pH 7.4) with and without 1.0 mM H_2O_2.

pH/ROS Dual-Sensitive Drug Release Behaviors

Oral drug delivery systems must be able to resist multiple challenges in the entire GI tract, especially the varied pH values. Therefore, the prepared nanosystems were exposed to SGF (pH 1.2), SIF (pH 6.8) and SCF (pH 7.4) to evaluate the drug release behaviors. Figure 6A presents the release profiles of DM from COC-DM and ACOC-DM, when exposed sequentially to SGF and SIF. In the first 2 h in SGF, DM was released slowly, with the cumulative release rate of 8.5 ± 4.1% for COC-DM and 5.5 ± 3.6% for ACOC-DM. During incubation of 2−12 h in SIF, drug release from the nanosystems gradually increased in a sustained manner, and DM release from ACOC-DM was considerably slower than that from COC-DM. The cumulative release rate reached 53.7 ± 3.0% for COC-DM and 30.6 ± 3.8% for ACOC-DM after 12 h of incubation. Moreover, a higher DM release rate of nanosystems was found in SCF relative to that in SIF, which reached 50.1 ± 2.2% for COC-DM and 35.1 ± 3.0% for ACOC-DM after only 4 h of incubation (Figure 6B). These results suggest that the drug release from the nanosystems is pH-dependent, which increases with increasing pH. This pH-sensitive release behavior of these nanosystems is probably due to the attenuated electrostatic interactions between the carbohydrates at higher pH, as the deprotonation of amino groups in CS. To evaluate the ROS-responsive drug release capacity, the nanosystems were additionally incubated in SCF (pH 7.4) with 1.0 mM H_2O_2. As shown in Figure 6B, in the presence of 1.0 mM of H_2O_2, both COC-DM and ACOC-DM showed substantially faster drug release than that in SCF without H_2O_2. More than 85% of DM was released from the nanosystems in a stimuli-responsive manner after incubation for 12 h, verifying the ROS-responsive drug release profile of the nanosystems due to the hydrolysis of the hydrophobic PBAP chains of OX-CD component.

As potential carriers for colon-specific delivery, CS and AHP have the ability to remain intact in the upper GI tract, but be specifically degraded by colonic flora. We expected that these carbohydrate-based nanosystems could sufficiently protect the incorporated labile drugs and minimize non-specific drug release before arriving in the colon. Drug release results demonstrate that the ACOC-DM with remarkable pH/ROS sensitivity could more efficiently prevent the premature drug release in the stomach and small intestines, and retain the entrapped drug until reaching the inflamed colon, compared to COC-DM. Together with the results of stability, dual-polysaccharide nanosystem ACOC-DM could not only improve the stability, but also improve the effectiveness of colitis-specific drug delivery than the single-polysaccharide nanosystem COC-DM, which provide a promising colon-specific delivery system for the enhanced oral drug delivery to treat UC.

Cellular Uptake and in vitro Anti-Inflammatory Activity

The cellular uptake and anti-inflammatory activity of two nanosystems were further compared in LPS-stimulated RAW 264.7 macrophages. Prior to commencing the anti-inflammatory activity study, cytotoxicity of these nanosystems was evaluated by means of MTT assay on human colorectal adenocarcinoma Caco-2 cells and RAW 264.7 macrophages, respectively. Figure 7A and B indicate that the cell viability of both Caco-2 cells and RAW 264.7 macrophages was

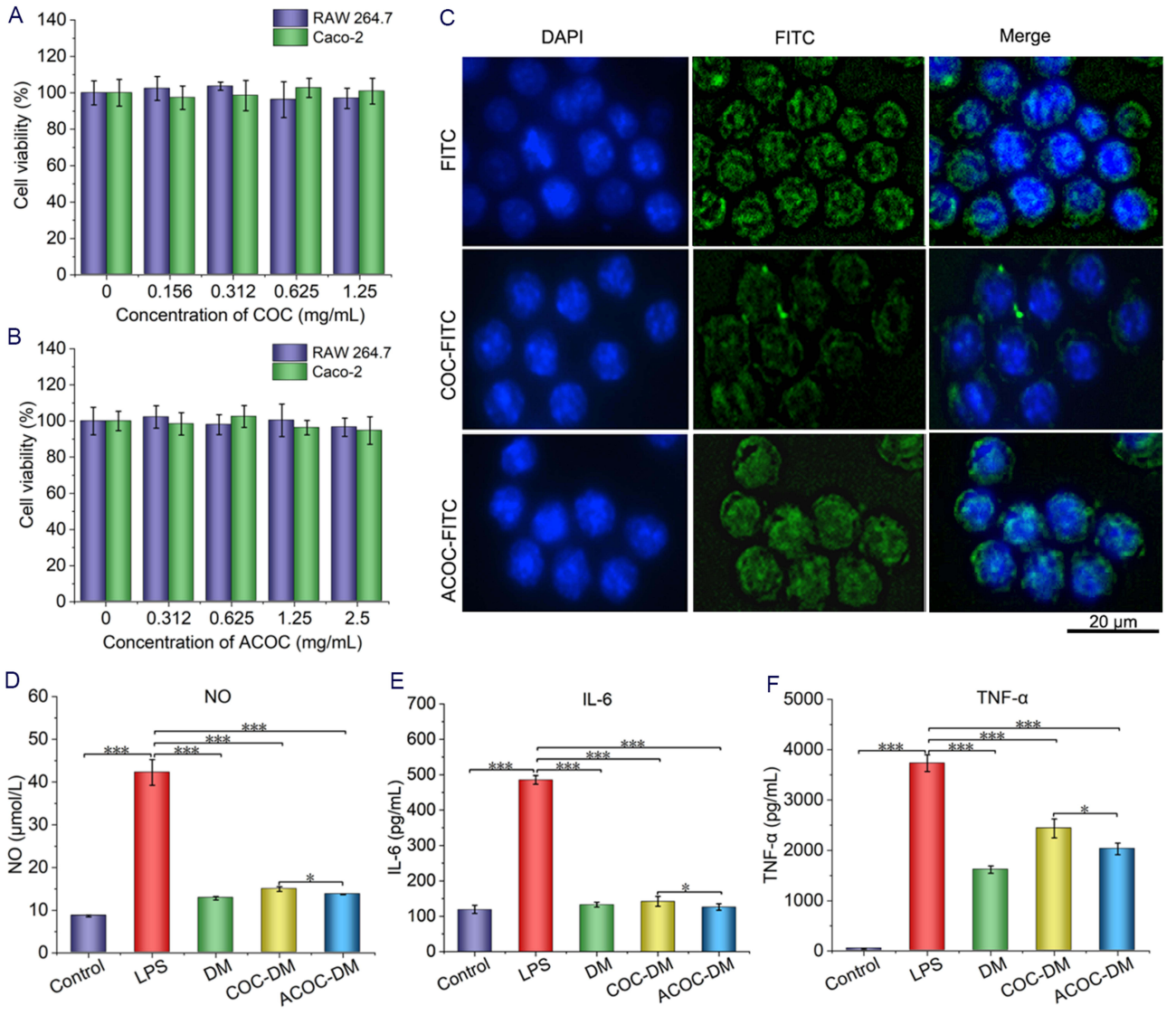

Figure 7 Cytotoxicity, cellular uptake and anti-inflammation effects on cells. Cytotoxicity of (**A**) COC and (**B**) ACOC in RAW 264.7 macrophages and Caco-2 cells. (**C**) Fluorescence imaging of RAW 264.7 macrophages treated with free FITC, COC-FITC and ACOC-FITC. (**D**) NO, (**E**) IL-6 and (**F**) TNF-α levels in LPS-stimulated RAW 264.7 macrophages treated with free DM, COC-DM and ACOC-DM. Results are expressed as the mean ± SD (n = 4, * $p < 0.05$ and *** $p < 0.001$).

higher than 95% after incubation with COC (0.156–1.25 mg/mL) or ACOC (0.312–2.5 mg/mL) for 24 h, suggesting the minimal cytotoxicity of these carbohydrate-based nanosystems. In Figure 7C, it was observed that the green fluorescence of ACOC-FITC incubated RAW 264.7 macrophages was similar to that observed in free FITC incubated macrophages but was much brighter than that of COC-FITC incubated macrophages, implying the higher cellular uptake of ACOC by macrophages. Figure 7D–F indicate that the secretion of NO, IL-6 and TNF-α was dramatically elevated upon stimulation with LPS. In contrast, both COC-DM and ACOC-DM significantly decreased LPS-stimulated NO, IL-6 and TNF-α secretion. Furthermore, it was noted that macrophages treated with ACOC-DM secreted lower levels of NO, IL-6, and TNF-α than those treated with COC-DM. These results demonstrate that ACOC-DM possess better anti-inflammatory activity than COC-DM ($p < 0.05$), which is in accordance with the findings of cellular uptake.

Physicochemical properties of polymeric nanoparticles, such as size and surface charges exert a significant influence on the cellular uptake and clearance of nanoparticles.[39] Phagocytic cell-mediated cellular internalization is mostly involved with engulfing the larger particles, since larger particles might coalesce within the cell membrane into a spherical structure that could be phagocytized quickly.[40] Surface charge is another dominant factor in cellular uptake.

Phagocytosis can be increased with increasing zeta potentials of both negatively and positively charged particles and was the lowest when zeta potential of particles was zero.[41] He et al reported that chitosan nanoparticles with high surface charge (either positive or negative) and large particle size were phagocytized more efficiently by murine macrophage.[42] Our results indicate that ACOC-DM had a larger particle size (538.32 ± 22.9 nm) in comparison to COC-DM with a smaller size (320.68 ± 8.16 nm). Moreover, ACOC-DM had a slightly higher negative potential (−15.46 ± 2.31 mV) than COC-DM (−11.82 ± 2.48 mV) in the DMEM medium. The larger size and higher potential of ACOC-DM facilitate the internalization into macrophages, resulting in the stronger anti-inflammatory activities. These findings further confirmed that the dual-polysaccharide nanosystem could enhance the uptake of macrophages and accumulate higher amounts of drug inside the cells, as compared to the single-polysaccharide nanosystem.

Bio-Distribution of Nanosystems in DSS-Induced Acute Colitis Mice

Having confirmed the superiority of dual-polysaccharide nanosystem over single-polysaccharide nanosystem in vitro, dual-polysaccharide nanosystem was further investigated in UC mice. In vivo fluorescent imaging was performed to track the bio-distribution of nanosystems in UC mice. ACOC-Cy-Cl were constructed following the same protocol used to generate ACOC-DM, except that DM was replaced with a near infrared probe Cy-Cl. DSS-induced UC mice were treated with ACOC-Cy-Cl or free Cy-Cl via oral administration, and then imaged upon NIR light excitation. As shown in Figure 8A, free Cy-Cl was rapidly absorbed from the GI tract after intragastric administration, and obvious fluorescent signals of Cy-Cl could be detected outside the GI tract till to 24 h post-administration, since free Cy-Cl was distributed throughout the body. Compared to free CyCl, ACOC-Cy-Cl rapidly moved from the upper GI tract to the lower segment within 4 h post-administration. No obvious fluorescence signal was observed outside the GI tract within 24 h after oral administration, indicating that ACOC-CyCl was mainly distributed in the GI tract.

Bio-distribution of Cy-Cl in the blood, isolated colon and main organs (heart, liver, spleen, lung and kidney) was further monitored by fluorescence imaging. The fluorescence intensity of free Cy-Cl in the blood was significantly lower in the ACOC-Cy-Cl group than that in the free Cy-Cl group (Figure 8B). The colon tissues of ACOC-Cy-Cl-treated mice exhibited much higher fluorescence intensity compared to that of free Cy-Cl treated mice at 4–8 h post-administration (Figure 8C). Fluorescent signals of Cy-Cl could also be detected in the main organs within 4–8 h in the free Cy-Cl group. In contrast, only weak fluorescence appeared in liver and lungs within 4–6 h in the ACOC-Cy-Cl group (Figure 8D).

The charged nanosystems can specifically target inflammatory tissues with opposite charge through electrostatic interaction. Unlike the healthy colon, the inflamed colonic mucins comprises negatively charged carbohydrate fractions, and some cationic charged proteins (eg transferrin, eosinophil cationic proteins) are abundant in the inflamed colon. Previous reports have demonstrated that negatively charged nanosystems give preferential adhesion to the cationic proteins in the inflamed colon, and enhance mucus penetration due to the electrostatic repulsion interaction.[11] For instance, Jubeh et al found that negatively charged liposomes exhibited a higher accumulation in the inflammatory regions than cationic or neutral charged liposomes.[43] Kotla et al reported that a negatively charged nanosystem (−31 mV) comprising with a PLGA core and a CS/hyaluronic acid (HA) shell displayed preferential adhesion onto a cationic charge surface of the inflamed colon, evidenced both in animal models and colon tissue biopsies from colitis patients.[3] Our results demonstrate that the strong negatively charged ACOC may facilitate the specific delivery of drugs to the inflamed colon, improve the drug accumulation in colitis tissues, and reduce the drug content entering the system circulation, thereby alleviating the systemic toxic and side effects.

Therapeutic Efficacy on DSS-Induced Acute Colitis Mice

Given that orally administered ACOC have the ability to preferentially accumulate in the inflamed colon of mice and release their payload in pH and ROS-dependent manners, it is reasonable to speculate that ACOC may serve as a promising drug delivery system for the targeted treatment of UC. We further evaluated the therapeutic efficacy of ACOC-DM and compared it to that of free DM in the DSS-induced colitis mice. Figure 9A shows the animal modeling and drug administration process. On day 10, the mice were euthanized and characterized for colitis phenotype. As depicted in Figure 9B–D, mice treated with DSS showed significant body weight loss (approximately 28%) and the colon length shortened to 3.6 ± 0.3 cm after 10 days ($p < 0.001$), compared to the control group with body weight gain of 7%

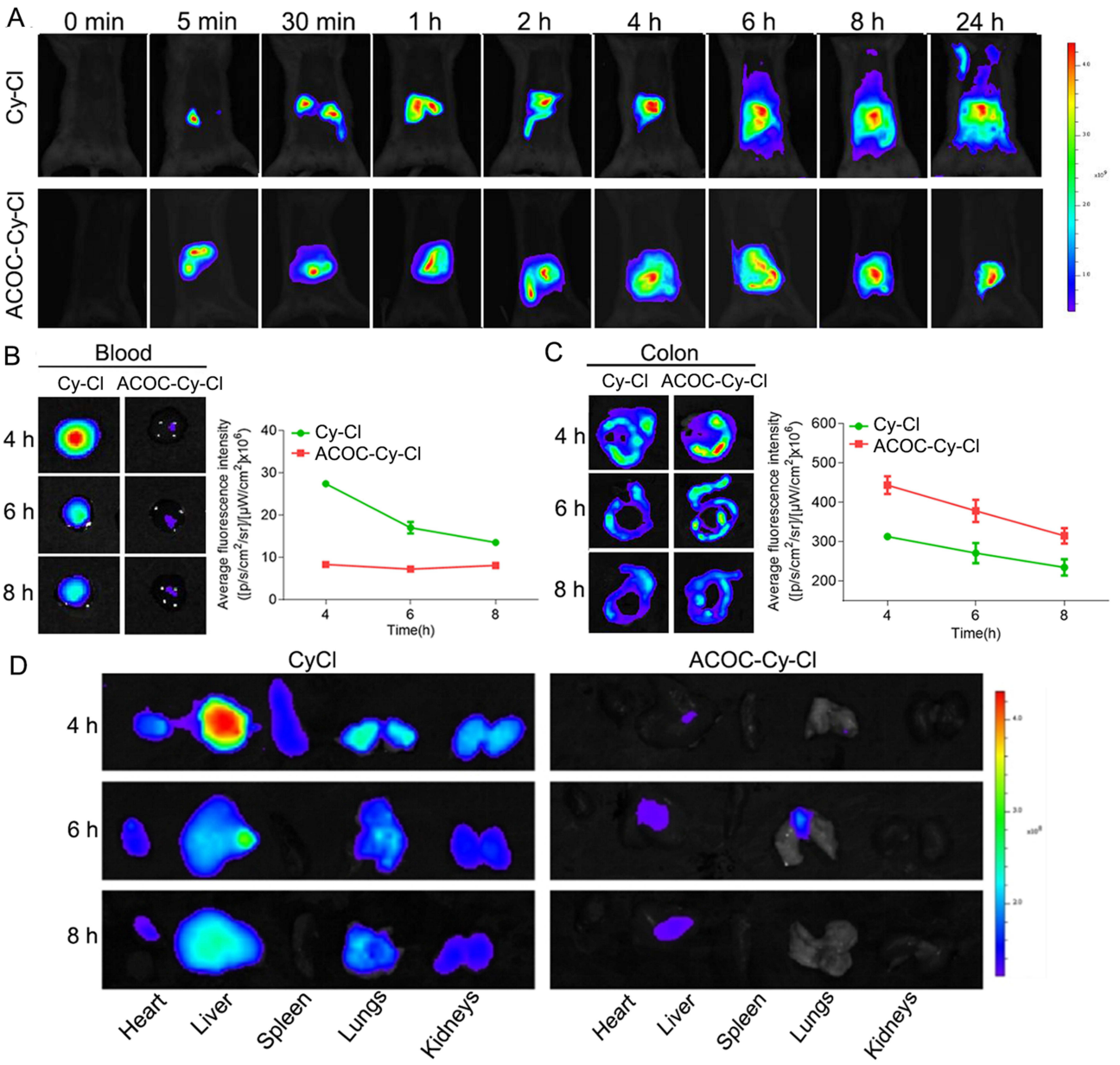

Figure 8 Bio-distribution of Cy-Cl labeled nanosystem in the UC mice. (**A**) Near-infrared imaging of the UC mice after oral administration of free Cy-Cl and ACOC-Cy-Cl at different time points (λex=700 nm, λem=790 nm). (**B**) Fluorescence imaging and intensity of Cy-Cl in the blood samples of free Cy-Cl and ACOC-Cy-Cl treated mice. (**C**) Fluorescence imaging and intensity of Cy-Cl in the colon tissues of free Cy-Cl and ACOC-Cy-Cl treated mice. (**D**) Fluorescence imaging of the major organs (heart, liver, spleen, lungs and kidneys) isolated from the free Cy-Cl and ACOC-Cy-Cl treated mice.

and colon length of 9.3 ± 0.7 cm, suggesting the successful establishment of the UC model. Compared to the DSS group, after receiving ACOC-DM treatment, the body weight loss and colon length shortening caused by DSS were dose-dependently attenuated at DM doses of 0.1, 0.25 and 0.5 mg/kg/d. ACOC-DM treatment effectively improved the symptoms of diarrhoea and bloody stools of UC mice. There was no significant difference in body weight loss (13% and 11%, respectively) and colon length (7.3 ± 0.5 cm and 7.4 ± 0.6 cm, respectively) between the ACOC-DM-0.25 group (DM dose of 0.25 mg/kg/d) and DM-0.5 group (DM dose of 0.5 mg/kg/d). Moreover, the body weight of the ACOC-DM-0.5 group nearly recovered to its initial levels on day 10, and the colon length increased to 8.5 ± 0.6 cm, which showed a remarkable difference compared to the DM-0.5 group. Similar differences were observed for DAI scores (Figure 9E). On day 10, the DAI score in the ACOC-DM-0.5 group was significantly lower than that in the free DM group and the DSS model group, which suggested the better anti-inflammatory effects of ACOC-DM. Additionally, the liver and spleen

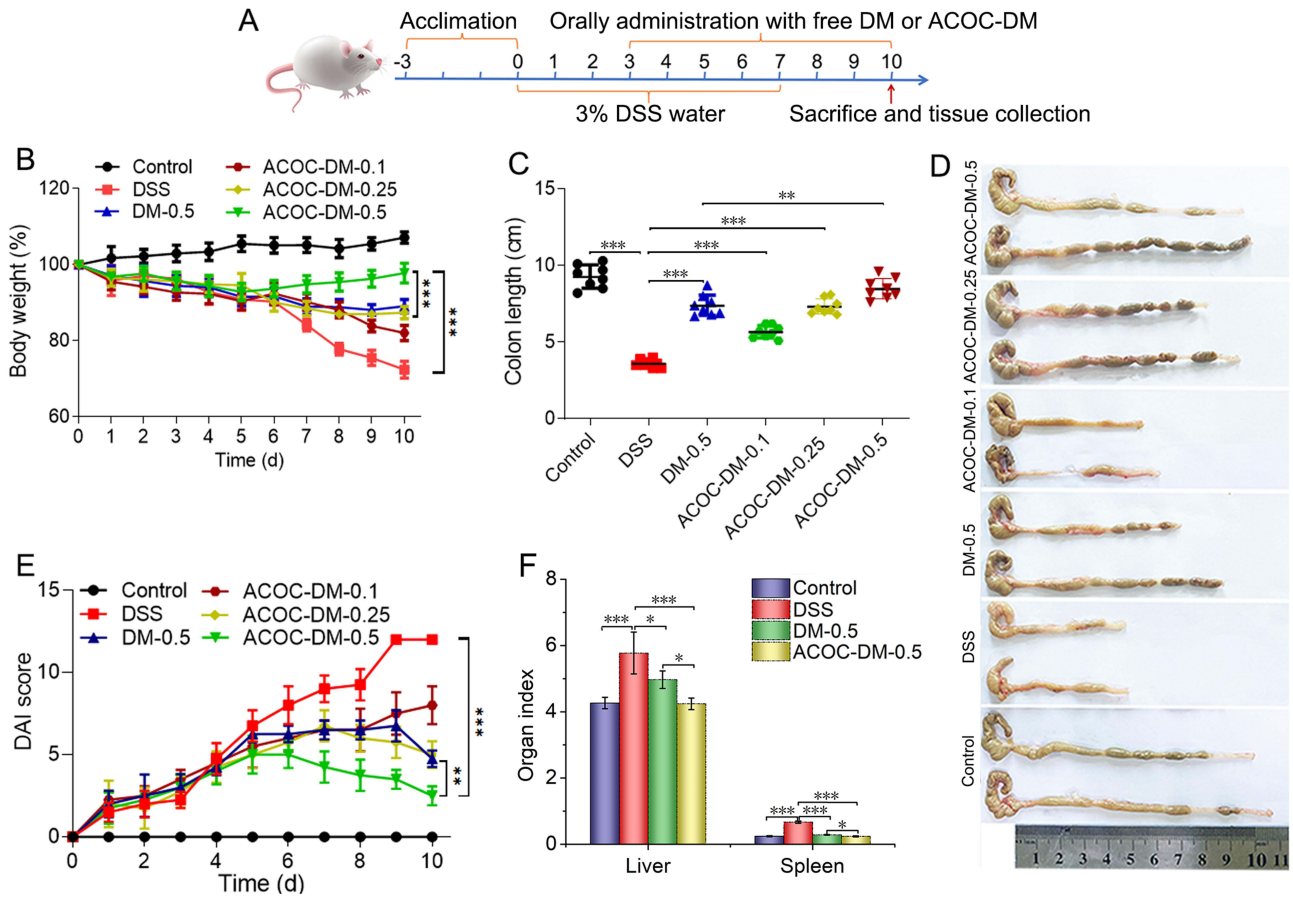

Figure 9 Therapeutic effects of ACOC-DM on the DSS induced UC mice. (**A**) Experimental scheme for UC treatment. (**B**) Body weight, (**C**) colon length, (**D**) photographs of the colon, (**E**) DAI score and (**F**) liver and spleen organ index of the UC mice in different treatment groups. *$p < 0.05$, **$p < 0.01$,***$p < 0.001$.

indexes of the DSS-induced mice were significantly higher than those of the control group (Figure 9F, $p < 0.001$), as mice with DSS-induced colitis appeared abnormal hepatosplenomegaly.[44] After treatment, the liver and spleen indexes of ACOC-DM-0.5 group were similar to those of the control group, but lower than those of the DM-0.5 group ($p < 0.05$), indicating that ACOC-DM has superior effects on UC treatment than free DM at the same dose.

To further compare the therapeutic efficacy of ACOC-DM and free DM, the levels of major pro-inflammatory cytokines associated with UC were evaluated in colonic tissues. As displayed in Figure 10A–C, the levels of colonic IL-6, IL-1β and TNF-α were all significantly inhibited in both the ACOC-DM-0.5 and DM-0.5 groups, compared to the DSS group ($p < 0.001$), indicating a reduction in colonic inflammation. Notably, the inhibitory effect of ACOC-DM on pro-inflammatory cytokines production was markedly greater than that of free DM at the same DM dose ($p < 0.001$). Colonic MPO and H_2O_2 serving as markers of oxidative stress were also measured. Figure 10D and E indicate that ACOC-DM treatment could more effectively reduce the elevated MPO activity and H_2O_2 production in the colon caused by DSS, compared to free DM at the same dose ($p < 0.001$). H&E staining was employed to assess the inflammatory damage to colon tissue (Figure 10F). It was observed that the colonic tissue in the DSS group had obvious mucosal ulceration, epithelium disruption, tissue edema, distorted crypt structure and significant inflammatory cell infiltration. However, ACOC-DM and free DM treatment effectively alleviated DSS-induced histopathological changes in colon tissue to varying degrees. The colonic tissue in the ACOC-DM-0.5 group almost maintained similar morphology to the control group. Taken together, these results indicate that the therapeutic efficacy of ACOC-DM is superior to that of free DM at the same dose in UC mice, since the dual-polysaccharide nanosystem with excellent pH/ROS sensitive release and UC-targeting ability could facilitate specific drug accumulation at inflammatory sites in the colon and reduce systemic side effects.

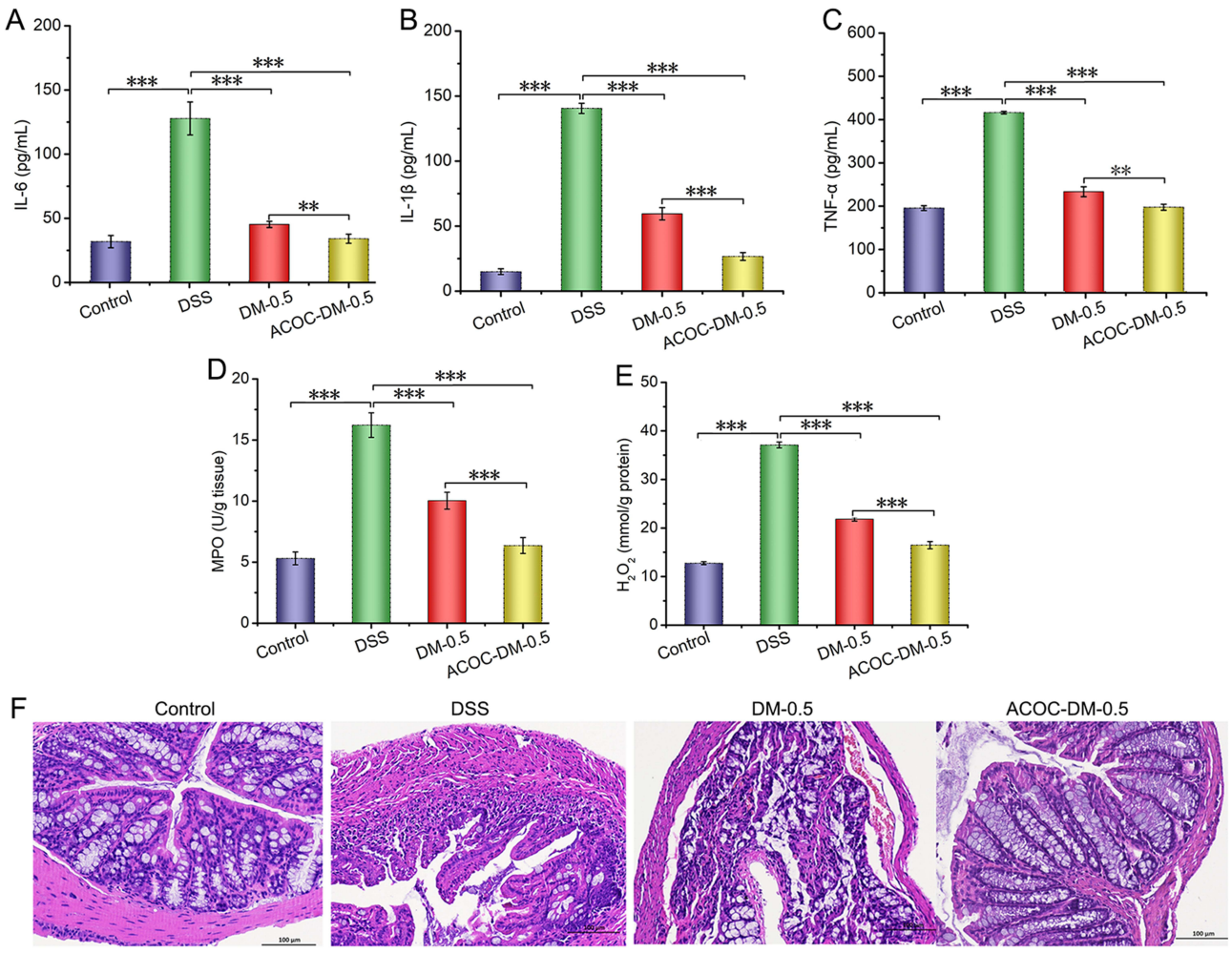

Figure 10 The levels of (**A**) IL-6, (**B**) IL-1β, (**C**) TNF-α, (**D**) MPO and (**E**) H_2O_2 in colon tissues of mice. (**F**) Histological sections of the colon tissues stained with hematoxylin and eosin (H&E) after different treatments. Data are shown as means ± SD. $^{**}p < 0.01$,$^{***}p < 0.001$.

Conclusion

In summary, pH/ROS dual-sensitive nanosystems were successfully fabricated using different kinds of carbohydrates that could be easily assembled by electrostatic interaction. The dual polysaccharide-coated ACOC-DM could effectively package DM and maintain their stability under the GI environments. In response to the variable pH and a high ROS level, ACOC-DM could specifically release drug in the inflammatory colon. By enhancing cellular uptake, ACOC-DM showed more effective anti-inflammatory efficacy compared to single polysaccharide-coated COC-DM in RAW 264.7 macrophages. After oral administration, effective localization of ACOC-DM at the inflammatory colon could be achieved by charge-mediated targeting effect. Furthermore, ACOC-DM responsive to the inflammatory microenvironment could more potently attenuate DSS-induced UC in mice than free DM. Consequently, this carbohydrate-based bioresponsive nanosystem holds promising potential for targeted drug delivery to potentiate the therapeutic efficacy of UC.

Acknowledgments

This work was supported by the Scientific and Technologic Foundation of Jilin Province [grant number 20210401060YY] and the Jilin Province Development and Reform Commission [grant number 2021C041-2]. The authors thank Dr. Mingzhou Sun, Northeast Normal University, for specimen identification.

Disclosure

The authors report no conflicts of interest in this work.

References

1. Jairath V, Feagan BG. Global burden of inflammatory bowel disease. *Lancet Gastroenterol*. 2020;5(1):2–3.
2. Neurath MF. Current and emerging therapeutic targets for IBD. *Nat Rev Gastroenterol Hepatol*. 2017;14(5):269–278. doi:10.1038/nrgastro.2016.208
3. Kotla NG, Singh R, Baby BV, et al. Inflammation-specific targeted carriers for local drug delivery to inflammatory bowel disease. *Biomaterials*. 2022;281:121364. doi:10.1016/j.biomaterials.2022.121364
4. Wang CPJ, Byun MJ, Kim SN, et al. Biomaterials as therapeutic drug carriers for inflammatory bowel disease treatment. *J Control Release*. 2022;345:1–19. doi:10.1016/j.jconrel.2022.02.028
5. Avallone EV, Pica R, Cassieri C, Zippi M, Paoluzi P, Vernia P. Azathioprine treatment in inflammatory bowel disease patients: type and time of onset of side effects. *Eur J Gastroen Hepat*. 2014;18(2):165–170.
6. Maltese P, Palma L, Sfara C, et al. Glucocorticoid resistance in Crohn's disease and ulcerative colitis: an association study investigating GR and FKBP5 gene polymorphisms. *Pharmacogenomics J*. 2012;12(5):432–438. doi:10.1038/tpj.2011.26
7. Quezada SM, McLean LP, Cross RK. Adverse events in IBD therapy: the 2018 update. *Expert Rev Gastroent*. 2018;12(12):1183–1191. doi:10.1080/17474124.2018.1545574
8. Kotla NG, Rana S, Sivaraman G, et al. Bioresponsive drug delivery systems in intestinal inflammation: state-of-The-art and future perspectives. *Adv Drug Deliv Rev*. 2019;146:248–266. doi:10.1016/j.addr.2018.06.021
9. Li Q, Lin L, Zhang C, et al. The progression of inorganic nanoparticles and natural products for inflammatory bowel disease. *J Nanobiotechnol*. 2024;22(1):17. doi:10.1186/s12951-023-02246-x
10. Deng C, Zhang H, Li Y, et al. Exosomes derived from mesenchymal stem cells containing berberine for ulcerative colitis therapy. *J Colloid Interf Sci*. 2024;671:354–373. doi:10.1016/j.jcis.2024.05.162
11. Chen F, Liu Q, Xiong Y, et al. Current strategies and potential prospects of nanomedicine-mediated therapy in inflammatory bowel disease. *Int J Nanomed*. 2021;16:4225–4237. doi:10.2147/IJN.S310952
12. Chen M, Lan H, Jin K, Chen Y. Responsive nanosystems for targeted therapy of ulcerative colitis: current practices and future perspectives. *Drug Deliv*. 2023;30(1):2219427. doi:10.1080/10717544.2023.2219427
13. Pu Y, Fan X, Zhang Z, et al. Harnessing polymer-derived drug delivery systems for combating inflammatory bowel disease. *J Control Release*. 2023;354:1–18. doi:10.1016/j.jconrel.2022.12.044
14. Jin T, Lu H, Zhou Q, et al. H_2S-releasing versatile montmorillonite nanoformulation trilogically renovates the gut microenvironment for inflammatory bowel disease modulation. *Adv Sci*. 2024;11(14):2308092. doi:10.1002/advs.202308092
15. Cui M, Zhang M, Liu K. Colon-targeted drug delivery of polysaccharide-based nanocarriers for synergistic treatment of inflammatory bowel disease: a review. *Carbohyd Polym*. 2021;272:118530. doi:10.1016/j.carbpol.2021.118530
16. Yang W, Zhao P, Li X, Guo L, Gao W. The potential roles of natural plant polysaccharides in inflammatory bowel disease: a review. *Carbohyd Polym*. 2022;277:118821. doi:10.1016/j.carbpol.2021.118821
17. Wei W, Zhang Y, Li R, et al. Oral delivery of pterostilbene by L-arginine-mediated "nano-bomb" carrier for the treatment of ulcerative colitis. *Int J Nanomed*. 2022;17:603–616. doi:10.2147/IJN.S347506
18. Hadji H, Bouchemal K. Advances in the treatment of inflammatory bowel disease: focus on polysaccharide nanoparticulate drug delivery systems. *Adv Drug Deliv Rev*. 2022;181:114101.
19. Ferreira LM, Dos Santos AM, Boni FI, et al. Design of chitosan-based particle systems: a review of the physicochemical foundations for tailored properties. *Carbohyd Polym*. 2020;250:116968.
20. Shah BM, Palakurthi SS, Khare T, Khare S, Palakurthi S. Natural proteins and polysaccharides in the development of micro/nano delivery systems for the treatment of inflammatory bowel disease. *Int J Biol Macromol*. 2020;165:722–737. doi:10.1016/j.ijbiomac.2020.09.214
21. Hua S, Marks E, Schneider JJ, Keely S. Advances in oral nano-delivery systems for colon targeted drug delivery in inflammatory bowel disease: selective targeting to diseased versus healthy tissue. *Nanomed-Nanotechnol*. 2015;11(5):1117–1132. doi:10.1016/j.nano.2015.02.018
22. Oshi MA, Naeem M, Bae J, et al. Colon-targeted dexamethasone microcrystals with pH-sensitive chitosan/alginate/Eudragit S multilayers for the treatment of inflammatory bowel disease. *Carbohyd Polym*. 2018;198:434–442. doi:10.1016/j.carbpol.2018.06.107
23. Xu Y, Zhu BW, Sun R, Li X, Wu D, Hu JN. Colon-targeting angelica sinensis polysaccharide nanoparticles with dual responsiveness for alleviation of ulcerative colitis. *ACS Appl Mater Interfaces*. 2023;15(22):26298–26315. doi:10.1021/acsami.3c02128
24. Xu Q, He C, Xiao C, Chen X. Reactive oxygen species (ROS) responsive polymers for biomedical applications. *Macromol Biosci*. 2016;16(5):635–646. doi:10.1002/mabi.201500440
25. Bertoni S, Liu Z, Correia A, et al. pH and reactive oxygen species-sequential responsive nano-in-micro composite for targeted therapy of inflammatory bowel disease. *Adv Funct Mater*. 2018;28(50):1806175. doi:10.1002/adfm.201806175
26. Huang L, Wang J, Kong L, et al. ROS-responsive hyaluronic acid hydrogel for targeted delivery of probiotics to relieve colitis. *Int J Biol Macromol*. 2022;222:1476–1486. doi:10.1016/j.ijbiomac.2022.09.247
27. Qi S, Luo R, Han X, et al. pH/ROS dual-sensitive natural polysaccharide nanoparticles enhance "one stone four birds" effect of Rhein on ulcerative colitis. *ACS Appl Mater Interfaces*. 2022;14(45):50692–50709. doi:10.1021/acsami.2c17827
28. Zhang Q, Tao H, Lin Y, et al. A superoxide dismutase/catalase mimetic nanomedicine for targeted therapy of inflammatory bowel disease. *Biomaterials*. 2016;105:206–221. doi:10.1016/j.biomaterials.2016.08.010
29. Zhang C, Li Q, Shan J, et al. Multifunctional two-dimensional Bi_2Se_3 nanodiscs for anti-inflammatory therapy of inflammatory bowel diseases. *Acta Biomater*. 2023;160:252–264. doi:10.1016/j.actbio.2023.02.016
30. Zhang C, Li Q, Xing J, et al. Tannic acid and zinc ion coordination of nanase for the treatment of inflammatory bowel disease by promoting mucosal repair and removing reactive oxygen and nitrogen species. *Acta Biomater*. 2024;177:347–360. doi:10.1016/j.actbio.2024.02.015

31. Li X, Lu C, Yang Y, Yu C, Rao Y. Site-specific targeted drug delivery systems for the treatment of inflammatory bowel disease. *Biomed Pharmacother*. 2020;129:110486. doi:10.1016/j.biopha.2020.110486
32. Zhang S, Langer R, Traverso G. Nanoparticulate drug delivery systems targeting inflammation for treatment of inflammatory bowel disease. *Nano Today*. 2017;16:82–96. doi:10.1016/j.nantod.2017.08.006
33. Dutta P, Mukherjee K, Saha A, Das A, Badwaik HR, Giri TK. Colonic delivery of surface charge decorated nanocarrier for IBD therapy. *J Drug Deliv Sci Tec*. 2022;76:103754. doi:10.1016/j.jddst.2022.103754
34. Prasher P, Fatima R, Sharma M. Cationic polysaccharides: emerging drug delivery vehicle across the physiological mucus barrier. *Future Med Chem*. 2022;14(8):531–533. doi:10.4155/fmc-2021-0296
35. Peng X, Yang G, Fan X, Bai Y, Ren X, Zhou Y. Controlled methyl-esterification of pectin catalyzed by cation exchange resin. *Carbohyd Polym*. 2016;137:650–656. doi:10.1016/j.carbpol.2015.11.005
36. Yu Y, Cui L, Liu X, et al. Determining methyl-esterification patterns in plant-derived homogalacturonan pectins. *Front Nutr*. 2022;9:925050. doi:10.3389/fnut.2022.925050
37. Zhang D, Wei Y, Chen K, et al. Biocompatible reactive oxygen species (ROS)-responsive nanoparticles as superior drug delivery vehicles. *Adv Health Mater*. 2015;4(1):69–76. doi:10.1002/adhm.201400299
38. Wang Y, Sun Y, Yang J, et al. Interactions of surface-functionalized starch nanoparticles with pepsin and trypsin in simulated gastrointestinal fluids. *J Agric Food Chem*. 2020;68(37):10174–10183. doi:10.1021/acs.jafc.0c02820
39. Sadat S, Jahan S, Haddadi A. Effects of size and surface charge of polymeric nanoparticles on in vitro and in vivo applications. *J Biomater Nanobiotech*. 2016;7(02):91–108. doi:10.4236/jbnb.2016.72011
40. Zhao F, Zhao Y, Liu Y, Chang X, Chen C, Zhao Y. Cellular uptake, intracellular trafficking, and cytotoxicity of nanomaterials. *Small*. 2011;7(10):1322–1337. doi:10.1002/smll.201100001
41. Ahsan F, Rivas IP, Khan MA, Suárez AIT. Targeting to macrophages: role of physicochemical properties of particulate carriers—liposomes and microspheres—on the phagocytosis by macrophages. *J Control Release*. 2002;79(1–3):29–40. doi:10.1016/S0168-3659(01)00549-1
42. He C, Hu Y, Yin L, Tang C, Yin C. Effects of particle size and surface charge on cellular uptake and biodistribution of polymeric nanoparticles. *Biomaterials*. 2010;31(13):3657–3666. doi:10.1016/j.biomaterials.2010.01.065
43. Jubeh TT, Barenholz Y, Rubinstein A. Differential adhesion of normal and inflamed rat colonic mucosa by charged liposomes. *Pharm Res*. 2004;21(3):447–453. doi:10.1023/B:PHAM.0000019298.29561.cd
44. Xu Y, Zhu BW, Li X, Li YF, Ye XM, Hu JN. Glycogen-based pH and redox sensitive nanoparticles with ginsenoside Rh2 for effective treatment of ulcerative colitis. *Biomaterials*. 2022;280:121077. doi:10.1016/j.biomaterials.2021.121077